[논 문] 한국재료학회지
Korean J. Mater. Res.
Vol. 29, No. 8 (2019)

https://doi.org/10.3740/MRSK.2019.29.8.463

Comparative Investigation of Interfacial Characteristics between HfO_2/Al_2O_3 and Al_2O_3/HfO_2 Dielectrics on AlN/p-Ge Structure

Hogyoung Kim[1†], Hee Ju Yun[2], Seok Choi[2] and Byung Joon Choi[2]

[1]Department of Visual Optics, Seoul National University of Science and Technology (Seoultech), Seoul 01811, Republic of Korea
[2]Departmet of Materials Science and Engineering, Seoul National University of Science and Technology (Seoultech), Seoul 01811, Republic of Korea

(Received June 17, 2019 : Revised July 12, 2019 : Accepted August 6, 2019)

Abstract The electrical and interfacial properties of HfO_2/Al_2O_3 and Al_2O_3/HfO_2 dielectrics on AlN/p-Ge interface prepared by thermal atomic layer deposition are investigated by capacitance–voltage(C–V) and current–voltage(I–V) measurements. In the C–V measurements, humps related to mid-gap states are observed when the ac frequency is below 100 kHz, revealing lower mid-gap states for the HfO_2/Al_2O_3 sample. Higher frequency dispersion in the inversion region is observed for the Al_2O_3/HfO_2 sample, indicating the presence of slow interface states A higher interface trap density calculated from the high-low frequency method is observed for the Al_2O_3/HfO_2 sample. The parallel conductance method, applied to the accumulation region, shows border traps at 0.3~0.32 eV for the Al_2O_3/HfO_2 sample, which are not observed for the Al_2O_3/HfO_2 sample. I–V measurements show a reduction of leakage current of about three orders of magnitude for the HfO_2/Al_2O_3 sample. Using the Fowler-Nordheim emission, the barrier height is calculated and found to be about 1.08 eV for the HfO_2/Al_2O_3 sample. Based on these results, it is suggested that HfO_2/Al_2O_3 is a better dielectric stack than Al_2O_3/HfO_2 on AlN/p-Ge interface.

Key words HfO_2/Al_2O_3, mid-gap states, leakage current.

1. Introduction

Germanium(Ge) has attracted significant attention as a channel material for the next generation nanoelectronics due to its high carrier mobility.[1)] One big obstacle for realizing high performance Ge n-channel metal-oxide-semiconductor field-effect transistors(MOSFETs) is the thermodynamically unstable germanium oxide(GeO) on the Ge substrate,[2)] which is easily desorbed from the GeO_2/Ge substrate during the thermal process. The GeO volatilization to the air generates large amount of defects and traps at the GeO_2/Ge interface.[3,4)] Numerous approaches such as nitridation, sulfur passivation, GeO_2 passivation have been employed to passivate the Ge surface and thus, to improve the interfacial quality.[5)] Among them, GeO_2 showed a promising result as a passivation layer with very low interface state density of $\sim 10^{10}$ cm^{-2} eV^{-1}.[6)] However, GeO_2 has low conduction band offset of ~0.6 eV,[7)] which is very low to prevent the electron injection over the barrier and the direct tunneling through the GeO_2 layer.[8)]

The high-k dielectrics can be used as an effective GeO_2 capping layer that prevents GeO desorption from the GeO_2/Ge interface.[9)] High quality of GeO_2/Ge interface can be obtained when the inward diffusion of oxygen vacancy is suppressed,[10)] if not, can introduce defect states and degrade the device performance. According to the comparison of HfO_2, $LaGeO_x$, $HfGeO_y$, GeN_x, and Al_2O_3 as passivating gate dielectrics for Ge substrates, Li et al. also showed that a key role is to block oxygen vacancy diffusion through the GeO_2.[11)] They suggested that Al_2O_3 is most proper material for this role, being a diffusion barrier and having large band offsets. Based on the calculation, it was demonstrated that AlN has fewer vacancy states in the Ge bandgap than Al_2O_3 and was suggested that AlN is a better choice for Ge MOSFET from the view of border trap properties, oxygen vacancy diffusion barrier, and band offset.[12)] Ge surface nitridation

[†]Corresponding author
E-Mail : hogyoungkim@gmail.com (H. Kim, Seoultech)

© Materials Research Society of Korea, All rights reserved.
This is an Open-Access article distributed under the terms of the Creative Commons Attribution Non-Commercial License (http://creative-commons.org/licenses/by-nc/3.0) which permits unrestricted non-commercial use, distribution, and reproduction in any medium, provided the original work is properly cited.

has also been found to successfully reduce the interface defect density,[13,14] Therefore, AlN might passivate Ge or GeO_2 surface better than Al_2O_3.

It was shown that combination of excellent thermal stability and large bandgap of Al_2O_3 and high dielectric constant of HfO_2 produced better equivalent oxide thickness scalability with low interface state density on Ge than single HfO_2 layer.[15] In this respect, we employed a thin AlN as passivation layer on Ge and comparatively investigated the electrical properties of both HfO_2/Al_2O_3 and Al_2O_3/HfO_2 capping layers.

2. Experimental

Ga-doped, single side polished, Ge(100) wafers (thickness: 500 mm, resistivity: 0.01~0.1 ohm.cm) grown by Czochralski method were used in this work. The Ge wafer was first cut into small pieces and the samples were loaded into an thermal ALD chamber after cleaning process in a HCl:H_2O (1:1) solution. The temperature was ramped up to 350 °C to deposit 2.0 nm thick AlN layer using Trimethylaluminum(TMA) and NH_3 as precursors. Then the temperature was lowered down to 250 °C to deposit AlN protection layers with two different methods, (i) 1.0 nm thick Al_2O_3 was deposited first and then 2.0 nm thick HfO_2 was deposited(denoted as HfO_2/Al_2O_3) and (ii) 2.0 nm thick HfO_2 was deposited first and then 1.3 nm thick Al_2O_3 was deposited(denoted as Al_2O_3/HfO_2). Al_2O_3 and HfO_2 films were grown by using the precursors of TMA and Tetrakis(ethylmethylamino)hafnium (TEMA-Hf), respectively, and H_2O vapor was used as the oxidant. The thicknesses of the deposited films were measured using a FS-1 multi-wavelength ellipsometer. Metal-oxide semiconductor (MOS) capacitors were fabricated with an Al Schottky electrode(diameter: 500 mm, thickness: 50 nm) and a Pt back contact(thickness: 100 nm) in order to examine the electrical characteristics of the AlN/Ge interface. Capacitance–voltage(C–V) measurements were performed using a HP 4284A LCR meter and current–voltage(I–V) measurements were carried out with a Keithley 238 current source.

3. Results and Discussion

Fig. 1 shows the C–V curves measured at various frequencies. Below 100 kHz, the weak inversion humps are observed for two samples. The inset in Fig. 1(b) shows the normalized C–V data obtained from 500 kHz and 5 kHz. It is known that the hump area is proportional to the amount of mid-gap states.[16] The C–V hump area was obtained by integrating the region bounded by two C–V curves measured at 500 kHz and 5 kHz. The C–V hump areas(i.e., Q_{hump}) were estimated to be 3.41×10^{-7} and 5.41×10^{-7} C/cm^2, respectively, for the Al_2O_3/HfO_2 and HfO_2/Al_2O_3 samples. This indicates that the HfO_2/Al_2O_3 sample reduced the mid-gap states compared to the Al_2O_3/HfO_2 sample. In addition, higher frequency dispersion in the inversion region was observed for the Al_2O_3/HfO_2 sample. Strong dispersion in the inversion region observed for the nitrided Ge sample was associated with the presence

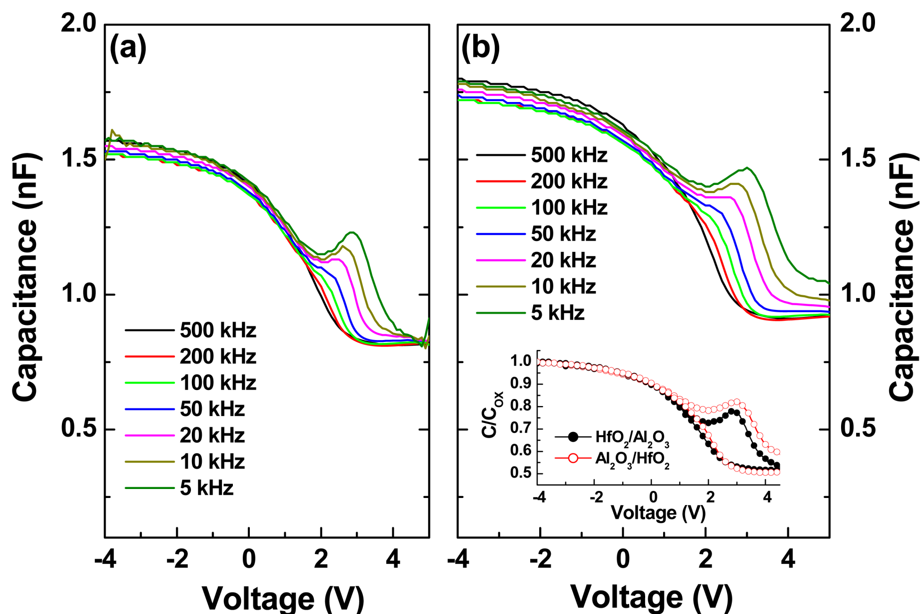

Fig. 1 Capacitance–voltage (C–V) data measured at various frequencies for the (a) HfO_2/Al_2O_3 and (b) Al_2O_3/HfO_2 samples. The inset in (b) shows the normalized capacitance values measured at 500 and 5 kHz.

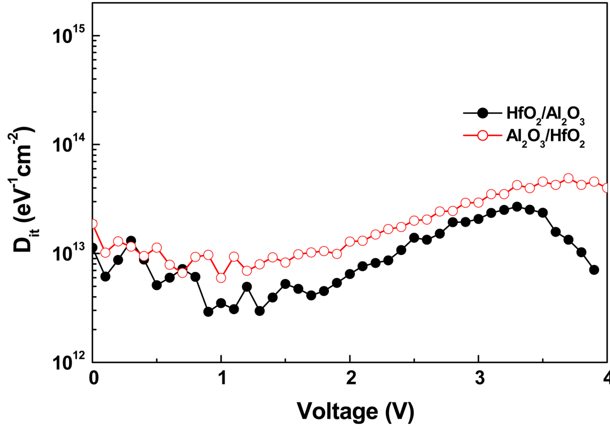

Fig. 2 Interface state density vs. voltage obtained from the high-low frequency method.

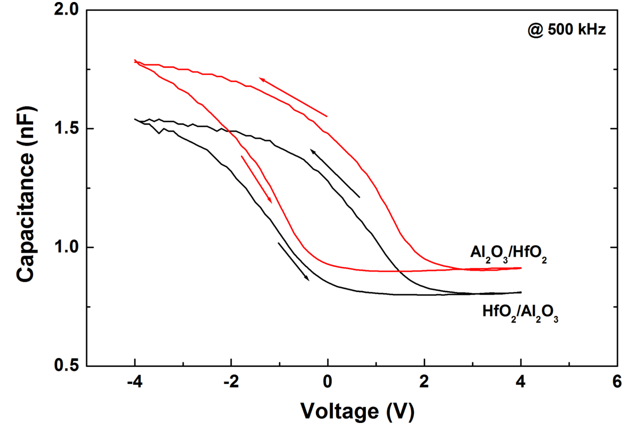

Fig. 3 C–V hysteresis plots measured at 500 kHz.

of slow interface states,[17] indicating the higher density of slow interface states for the Al_2O_3/HfO_2 sample.

Fig. 1 also shows that the accumulation capacitances are a little higher for the Al_2O_3/HfO_2 sample as compared to the HfO_2/Al_2O_3 sample. Al_2O_3 and HfO_2 have large bandgaps(7.0 and 5.7 eV, respectively) and high dielectric constants(~9 and ~20, respectively).[18] It was reported that the formation of Hf–Al–O by the intermixture of Al_2O_3 and HfO_2 layers provided the dielectric constant between 9 and 20.[19] The bonding energies of Al–O and Hf–O are known to be 501.9(± 10.6) and 801 (± 13) kJ/mol, respectively.[20] Hence, Al–O bonding would be dissolved more easily than Hf–O bonding. For the HfO_2/Al_2O_3 sample, the outdiffusion of Al atoms from the first-deposited Al_2O_3 layer might occur during the HfO_2 deposition, leading to the formation of Hf–Al–O and decreasing the effective dielectric constant of dielectric layers. For the Al_2O_3/HfO_2 sample, the outdiffusion of Hf atoms from the first-deposited HfO_2 layer might not occur well during the Al_2O_3 deposition due to the higher bonding energy of Hf–O, suppressing the formation Hf–Al–O and producing the relatively higher effective dielectric constant of dielectric layers. Due to the difference in the effective dielectric constant, the different capacitance values were obtained. However, further investigation using x-ray photoelectron spectroscopy measurements is required in order to confirm this explanation.

Based on high–low frequency method, the interface state density(D_{it}) across the band gap was extracted using the following equation[21]

$$D_{it} = \frac{C_{OX}}{q}\left[\frac{C_{Hf}/C_{OX}}{1-C_{Lf}/C_{OX}} - \frac{C_{Lf}/C_{OX}}{1-C_{Hf}/C_{OX}}\right] \tag{1}$$

where C_{OX} is the oxide capacitance at the accumulation, C_{Hf} and C_{Lf} are the capacitances at high and low frequencies. Here, C_{OX} values were obtained experimentally at 500 kHz from the accumulation region. In the calculation, 500 kHz and 1 kHz were selected as the high and low frequencies, respectively. Fig. 2 shows the D_{it} as a function of the gate voltage. Note that high-low frequency method can underestimate the D_{it} values because neither the 500 KHz nor the 1 kHz C–V data would be true high and low frequency curves, respectively. Nevertheless, this clearly shows that the HfO_2/Al_2O_3 sample has lower interface state density than the Al_2O_3/HfO_2 sample.

Fig. 3 shows the C–V hysteresis characteristics measured at 500 kHz. For both samples, a very large hysteresis was observed at the flat-band voltage(V_{FB}), indicating the presence of high density of bulk oxide traps.[22] The C–V hysteresis was also associated with the GeO volatilization,[20] which could produce large amount of defects and traps in the high-k film.[3] It is seen that the hysteresis C–V traces of both samples revealed the negative V_{FB} shift, implying the positive charge trapping. Hole injection from p-type Ge substrate and trapping under the negative gate bias occurred higher than electron trapping under the positive gate bias during C–V hysteresis measurements.[24] The average oxide trap densities (Q_T) along the Ge bandgap (E_g) were obtained through the relation $Q_T = (C_{OX}\Delta V_{FB})/qE_g$, where ΔV_{FB} is the flatband voltage shift. The Q_T values were calculated to be 1.39×10^{13} and 1.86×10^{13} $cm^{-2}eV^{-1}$, respectively, for the Al_2O_3/HfO_2 and HfO_2/Al_2O_3 samples.

Further investigation was performed by obtaining the parallel conductance values (G_p/ω) from the accumulation region.[25] G_p/ω values as a function of radial frequency ($\omega = 2\pi f$) were derived by $G_p/\omega = [\omega G_m(C_{OX})^2]/[(G_m)^2 + \omega^2(C_{OX} - C_m)^2]$, where C_m and G_m are the measured capacitance and conductance, respectively. These G_p/ω values can be connected with the following equation[26]

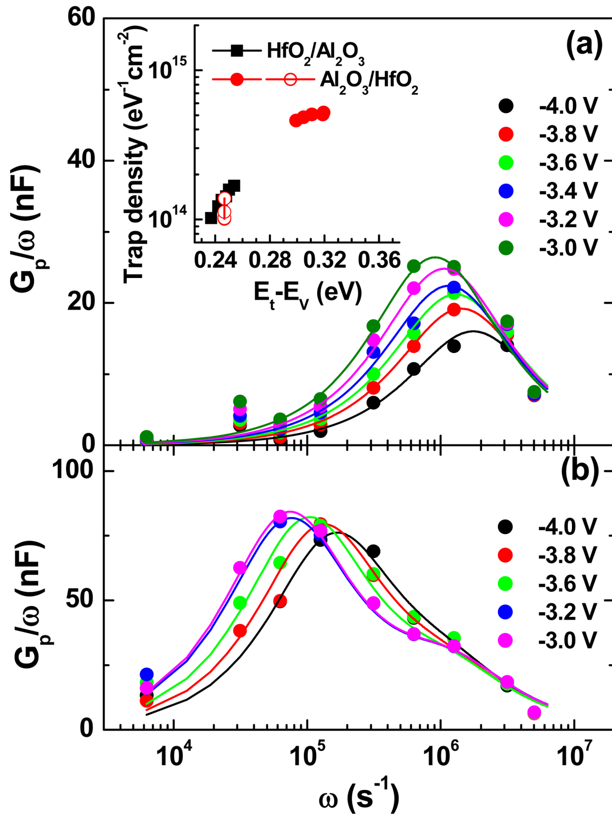

Fig. 4 Frequency dependent parallel conductance for the (a) HfO_2/Al_2O_3 and (b) Al_2O_3/HfO_2 samples. The inset in (a) shows the obtained trap densities from the conductance method.

$$\frac{G_p}{\omega} = \frac{q\omega\tau_T D_T}{1+(\omega\tau_T)^2} \tag{2}$$

where D_T is the trap density and τ_T is the trap response time. The experimental and fitting data are shown in Fig. 4. The measured curves for the HfO_2/Al_2O_3 and Al_2O_3/HfO_2 samples were resolved into one and two fitting curves, respectively. The energy level of traps above the Ge valence band, $E_t - E_V$ were determined from τ_T according to the Shockley-Read-Hall statistics[27]

$$E_t - E_V = kT\ln\left(\frac{\sigma_p v_{th} N_V}{\tau_T}\right) \tag{3}$$

where v_{th} is the thermal velocity, σ_p is the hole capture cross section ($\sim 1 \times 10^{-16}$ cm^2),[28] and N_V is the effective density of states in the Ge valence band. As shown in the inset in Fig. 4(a), the traps located at ~0.25 eV with the time constants between 0.5 and 1 µs were observed for both samples. These traps are likely to be located near the AlN/Ge interface. Meanwhile, the traps located at 0.3~0.32 eV observed for the Al_2O_3/HfO_2 sample, which is not observed for the HfO_2/Al_2O_3 sample. Because the time constants for these traps are 6~15 µs, they may be regarded as slow states. Border traps show a slower conductance response due to the time needed for the carriers to reach the traps within the AlN layer from the AlN/Ge interface. That is, these traps might be located within the AlN layer, which were generated during the HfO_2 deposition.

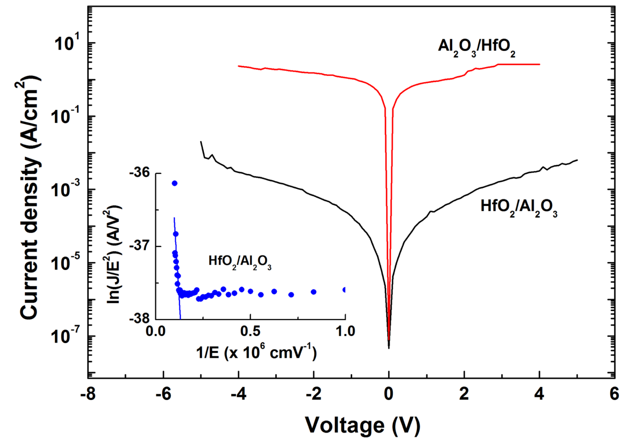

Fig. 5 Current density–voltage (J–V) characteristics at room temperature. The inset shows the Fowler–Nordheim (FN) tunneling plot of $\ln(J/E^2)$ versus 1/E for the HfO_2/Al_2O_3 sample.

The leakage current density as a function of the voltage is shown in Fig. 5. At accumulation region, the gate leakage recorded the values of 3×10^{-3} and 2.3 A/cm^{-2} at -4.0 V for the HfO_2/Al_2O_3 and Al_2O_3/HfO_2 samples, respectively. This figure demonstrates a reduction of leakage current for the HfO_2/Al_2O_3 sample by about three orders of magnitude, indicating again the better insulator quality. HfO_2 is known to suffer from poor thermal stability and low crystallization temperature(500°C), which produces large leakage current flowing along the grain boundary.[29] Thermal stability experiments using the HfO_2/Al_2O_3 bilayer in the AlGaN/GaN device have shown that improved device performance was due to the formation of the Hf–Al–O structure and the amorphous nature of the Al_2O_3 layer.[30] Miyazaki et al. observed the larger leakage current using the HfO_2 than that using the Al_2O_3 in the AlGaN/GaN device and they attributed this to the grain boundaries of the microcrystal in the HfO_2 acting as the leakage path.[31] The larger leakage current was also associated with a lower conduction band offset of 1.1 eV between HfO_2 and GaN than that of 2.3 eV between Al_2O_3 and GaN.[31,32] In addition, analysis of C–V characteristics of the HfO_2/AlN stacks on GaN confirmed the dielectric constant of the HfO_2 to be ~20, which is a typical value of ALD HfO_2.[33] This indicates

that the outdiffusion of Al atoms from the AlN layer into the HfO_2 layer was insignificant. As explained previously, the HfO_2/Al_2O_3 sample might form the Hf–Al–O bonding more easily than the Al_2O_3/HfO_2 sample. Based on these results, we can assume that the HfO_2 layer in the Al_2O_3/HfO_2 sample did not underwent significant intermixing. Hence, the grain boundaries of the microcrystal in the HfO_2 would not be affected in the Al_2O_3/HfO_2 sample, which caused a larger leakage current. Consequently, Al_2O_3 is a better choice than HfO_2 as the first deposition layer on AlN/p-Ge. As shown in the inset in Fig. 5, the forward bias current for the HfO_2/Al_2O_3 sample was analyzed using the Fowler-Nordheim(FN) emission, given by $J \propto E^2\exp(-\beta/E)$.[34] From the slope, the barrier height was calculated to be about 1.08 eV.

4. Conclusion

Using C–V and I–V measurements, we investigated the electrical and interfacial properties of HfO_2/Al_2O_3 and Al_2O_3/HfO_2 dielectrics on AlN/p-Ge interface. The inversion humps related to mid-gap states were observed for both samples, which was found to have lower mid-gap states for the HfO_2/Al_2O_3 sample. High-low frequency method revealed the lower interface trap density for the HfO_2/Al_2O_3 sample. According to the parallel conductance method applied to the accumulation region, the border traps at $0.3 \sim 0.32$ eV were observed for the Al_2O_3/HfO_2 sample, which was not observed for the HfO_2/Al_2O_3 sample. Therefore, it would be reasonable to assume that these traps were generated during the HfO_2 deposition. The reduction of leakage current by about three orders of magnitude was observed for the HfO_2/Al_2O_3 sample. These results clearly indicate the better insulator quality with an HfO_2/Al_2O_3 dielectric stack.

Acknowledgments

This work was supported by Basic Science Research Program through the National Research Foundation of Korea (NRF) funded by the Ministry of Education (2017R1D1A1B03030400).

References

1. P. Lim, D. Chi, X. Wang and Y. Yeo, Appl. Phys. Lett., **101**, 172103 (2012).
2. K. Prabhakaran, F. Maeda, Y. Watanabe and T. Ogino, Appl. Phys. Lett., **76**, 2244 (2000).
3. F. Bin, L. Xia, F. Xi, M. Fei, F. Jiao and H. Yue, Chin. Phys. B, **22**, 037702 (2013).4. Y. Seo, C. Kim, T. Lee, W. Hwang, H. Yu, Y. Choi and B. Cho, IEEE Trans. Electron Dev., **64**, 3998 (2017).
5. Q. Xie, S. Deng, M. Schaekers, D. Lin, M. Caymax, A. Delabie, X. Qu, Y. Jiang, D. Deduytsche and C. Detavernier, Semicond. Sci. Technol., **27**, 074012 (2012).
6. 4. Y. Fukuda, T. Ueno, S. Hirono and S. Hashimoto, Jpn. J. Appl. Phys., **44**, 6981 (2005).
7. M. Perego, G. Scarel, M. Fanciulli, I. Fedushkin and A. Skatova, Appl. Phys. Lett., **90**, 162115 (2007).
8. D. Kuzum, T. Krishnamohan, A. Nainani, Y. Sun, P. Pianetta, H. Wong and K. Saraswat, IEEE Trans. Electron Dev., **58**, 59 (2011).
9. R. Zhang, P.-C. Huang, J.-C. Lin, N. Taoka, M. Takenaka and S. Takagi, IEEE Trans. Electron Dev., **60**, 927 (2013).
10. D. Kuzum, T. Krishnamohan, A. Pethe, A. Okyay, Y. Oshima, Y. Sun, J. McVittie, P. Pianetta, P. McIntyre and K. Saraswat, IEEE Electron Dev. Lett., **29**, 328 (2008).
11. H. Li, L. Lin and J. Robertson, Appl. Phys. Lett., **101**, 052903 (2012).
12. H. Li, Y. Guo and J. Robertson, Microelectron. Eng., **147**, 168 (2015).
13. R. Zhang, T. Iwasaki, N. Taoka, M. Takenaka and S. Takagi, J. Electrochem. Soc., **158**, G178 (2011).
14. H. Kim, P. McIntyre, C. Chui, K. Saraswat and M. Cho, Appl. Phys. Lett., **85**, 2902 (2004).
15. X. Li, Y. Cao, A. Li, H. Li and D. Wu, ECS Solid State Lett., **1**, N10 (2012).
16. I. Krylov, L. Kornblum, A. Gavrilov, D. Ritter and M. Eizenberg, Appl. Phys. Lett., **100**, 173508 (2012).
17. D. Misra, Electrochem. Soc. Interface, **20**, 47 (2011).
18. M. Usman, C. Henkel and A. Hall´en, ECS J. Solid State Sci. Technol., **2**, N3087 (2013).
19. G. Wilk, M. Green, M. Ho, B. Busch, T. Sorsch, F. Klemens, B. Brijs, R. van Dover, A. Kornblit, T. Gustafsson, E. Garfunkel, S. Hillenius, D. Monroe, P. Kalavade and M. Hergenrother, Tech. Dig. VLSI Symp., p. 88 (2002).
20. J. Kerr, Strengths of Chemical bonds, in CRC Handbook of Chemistry and Physics, p. 9-54, ed. D. R. Lide, CRC Press, Boca Raton, FL (2005).
21. R. Engel-Herbert, Y. Hwang and S. Stemmer, J. Appl. Phys., **108**, 124101 (2010).
22. F. Bellenger, M. Houssa, A. Delabie, V. Afanasiev, T. Conard, M. Caymax, M. Meuris, K. Meyer and M. Heyns, J. Electrochem. Soc., **155**, G33 (2008).
23. Y. Choi, H. Lim, S. Lee, S. Suh, J. Kim, H. Jung, S. Park, J. Lee, S. Kim, C. Hwang and H. Kim, ACS. Appl, Mater. Interfaces, **4**, 7885 (2014)
24. H. Seo, F. Bellenger, K. Chung, M. Houssa, M. Meuris, M. Heyns and G. Lucovsky, J. Appl. Phys., **106**, 044909 (2009).
25. Y. Yuan, L. Wang, B. Yu, B. Shin, J. Ahn, P. McIntyre, P. Asbeck, M. Rodwell and Y. Taur, IEEE Electron Dev. Lett., **32**, 485 (2011).
26. D. Schroder, Semiconductor Material and Device Characterization, p. 1, Wiley, New York, USA (2005).

27. S. Gupta, E. Simoen, R. Loo, O. Madia, D. Lin, C. Merckling, Y. Shimura, T. Conard, J. Lauwaert, H. Vrielinck and M. Heyns, ACS Appl. Mater. Interfaces, **8**, 13181 (2016).
28. D. Wang, S. Kojima, K. Sakamoto, K. Yamamoto and H. Nakashima, J. Appl. Phys., **112**, 083707 (2012).
29. G. He, L. Zhang, G. Meng, G. Li, Q. Fang and J. Zhang, J. Appl. Phys., **102**, 094103 (2007).
30. F. Tian and E. Chor, J. Electrochem. Soc., **157**, H557 (2010).
31. E. Miyazaki, Y. Goda, S. Kishimoto and T. Mizutani, Solid-State Electron., **62**, 152 (2011).
32. J. Robertson and B. Falabretti, J. Appl. Phys., **100**, 014111 (2006).
33. D. Deen, S. Binari, D. Storm, D. Katzer, J. Roussos, J. Hackley and T. Gougousi, Electron. Lett., **45**, 423 (2009).
34. G. Dutta, N. DasGupta and A. DasGupta, IEEE Trans. Electron Dev., **64**, 3609 (2017).